



Optimization of LiFePO_4 cathode material based on phosphorus doped graphite network structure for lithium ion batteries

Chunlei Li^{1,2} · Yingchun Xie^{1,2} · Ningshuang Zhang^{1,2} · Ling Ai^{1,2} · Youwei Liang^{1,2} · Kuanyou Tuo^{1,2} · Xiushen Ye³ · Guofeng Jia³ · Shiyu Li^{1,2,3}

Received: 23 July 2018 / Revised: 5 September 2018 / Accepted: 22 September 2018 / Published online: 30 September 2018
© Springer-Verlag GmbH Germany, part of Springer Nature 2018

Abstract

Lithium iron phosphate (LiFePO_4) has been recommended as a hopeful cathode material for lithium ion batteries (LIBs) in the future due to its lots of advantages, such as stable operating voltage, excellent cycle performance, controllable cost, and environmental protection. However, pure LiFePO_4 (LFP) shows bad reversible capacity and charge/discharge performance at high rate. Many methods including decrease of particle size, optimization of coating carbon, introduction of conductive polymer, and doping of metal or non-metallic element have been developed to improve the electrochemical performance of LFP cathode material. In this study, LFP/C-P composite cathodes were prepared successfully by a facile sol-gel approach that graphite was used to generate a carbon network structure and triphenylphosphine was used to greatly facilitate generation of a network connecting passage. Electrochemical test results show that LFP/C-P composite cathode has achieved a remarkable improvement in capacity and apparent ascension in rate performance. Compared with LFP, LFP/C, and LFP-P cathode, LFP/C-P composite material shows the best electrochemical performance with a discharge capacity of 168.8 mAh g^{-1} and a remarkable retention rate of 98.8% over 100 cycles at 0.1 C.

Keywords Lithium ion battery · Cathode material · LFP · Phosphorus · Graphite · Network structure

Introduction

The electrochemical properties and application of lithium ion batteries (LIBs) are highly restricted by the performance of the cathode materials, which are the important key parameters regarding volumetric energy, power density, coulombic efficiency, cycle life, and cost of manufacture [1]. Recently, electric vehicles and hybrid electric vehicles have been attracted more attentions because of the rapid consumption of fossil fuels and greater environmental pollution caused by automobiles [2]. Today, LIBs are the main power sources for the

electric vehicles and hybrid electric vehicles because of the great reversible capacity, which can be greatly related to the outstanding cathode material. In addition, LIBs have potential applications in portable electronics and electric energy storage equipment. Currently, owing to the increasing demands for LIBs with high discharge capacity and prominent cyclic stability, there are tremendous efforts to strengthen the performance of electrochemical energy storage equipment [3].

Lithium iron phosphate (LiFePO_4) has been extensively researched as a most promising cathode material for LIBs attributed to its excellent cycle performance, superior theoretical capacity ($\sim 170 \text{ mAh g}^{-1}$), low cost, stable safety, and nontoxicity [4]. Nevertheless, the extensive application of pristine LiFePO_4 (LFP) is restricted by its intrinsic inferior electronic conductivity ($\sim 10^{-9} \text{ S cm}^{-1}$ at RT) and low diffusion coefficient ($\sim 10^{-11}$ – $10^{-9} \text{ S cm}^{-1}$ at RT) of Li^+ through the structure, which seriously obstructs the high rate capability of LIBs. To solve these serious defects, a series of modified measures have been proposed to enhance the performance of LFP, such as selectively doping with metal and non-metallic elements, coating with electronically conductive materials on the surface of LFP, optimizing LFP particle size, and

✉ Shiyu Li
sylimw@163.com

¹ College of Petrochemical Technology, Lanzhou University of Technology, Lanzhou 730050, China

² Gansu Engineering Laboratory of Cathode Material for Lithium-ion Battery, Lanzhou 730050, China

³ Qinghai Institute of Salt Lakes, Chinese Academy of Sciences, Xining 810008, China

controlling LFP crystal morphology [5]. As is known to all, LFP with a standardized orthorhombic structure belongs to the olivine family [6]. In addition, the PO_4 tetrahedron breaks the chains of FeO_6 octahedrons, which results in a low electronic conductivity [7]. Computational and experimental results indicate that LFP material has only one-dimensional (1D) bind channels resulting in slow Li^+ migration during the charge-discharge cycles. In fact, these channels are easily impeded by many impurities or defects, and thus lead to a lazy Li^+ diffusion process [8]. However, a successive network with FeO_6 cannot be achieved by the above proposed structure that leads to its low electronic conductivity [9]. On the basis of the special structure mentioned, how to overcome those major defects is the key to promote the electrochemical performance of LFP.

It is a question that how to improve Li^+ diffusion and enhance the electronic conductivity, in order to achieve a high capability of LFP. The combination of carbon coating and element doping is used widely in many past research results. Carbon coating can solve the defects of high impedance of LFP cathode material [10], because the even carbon layer aggraded on the surface of LFP can catch almost electrons from all different directions and boost the diffusion of Li^+ easily through the thin carbon layer with less polarization. Accordingly, some appropriate elements can be introduced into the lattice in order to decrease the gap between the conduction and valence bands [11, 12] and expand Li^+ diffusion pathway so that Li^+ can insert/deinsert easily at high rates. For instance, some elements (such as Al [13], Zr [14], and Mg [15]) have been doped into the materials to promote the electrochemical performance of LFP cathode material. Accordingly, doping phosphorus into the LFP/C mixture in a simple sol-gel way has led to a remarkable promotion of both conductivity and electrochemical performance of LFP material. Reportedly, the phenomenon can be attributed to the expanded path way of Li^+ diffusion [16, 17].

In addition, Wang et al. [18] synthesized LFP@N-doped carbon nanocomposite sample using polybenzoxazine as a novel carbon and nitrogen source, which expressed an excellent performance with a reversible discharge capacity of 132 mAh g^{-1} after 180 cycles at 2 C, which is equal to 93.2% of the initial value. For the moment, it has been studied widely that phosphorus doped into carbon structure improved the performance of LFP composite with C-O reaction [19, 20]. The research results encouraged the later researchers to investigate that how the phosphorus doping enhances the conductivity of the LFP composite with a carbon coating layer, which promotes a final formation of carbon network structure, thus ultimately results in LFP cathode material with a superior electrochemical performance [21].

In this work, several different forms of LFP, LFP-P, LFP/C, and LFP/C-P composites are synthesized in the sol-gel way to achieve optimal experiment conditions and obtain the best

discharge specific capacity and cycling ability. Especially, the effect of phosphorus doped graphite network structure on the electrochemical performance of LFP/C-P composite cathode materials is tested by many different electrochemical methods, including electrochemical impedance spectroscopy (EIS) tested through CHI660C electrochemical workstation (Shanghai, China), charge/discharge cycle processes carried out on a LAND CT2001A tester (Wuhan, China), and X-ray photoelectric spectroscopy (XPS) (GG 314-JPS-9200) measured by X-ray photoelectron spectroscopy techniques. Moreover, the distribution and content of elements are studied by EDX and elemental mapping. The crystalline phase and structure of the synthesized samples are researched by X-ray diffraction (XRD) performed by X-ray diffractometer (XRD, Rint-2000, Rigaku, Japan) using CuK α radiation over the 2θ range of 10° – 80° . And, the surface morphology and structure are observed by transmission electron microscopy (TEM, JEM-2100, JOEL, Japan) and scanning electron microscopy (SEM, JSM-5600, Japan).

Experimental sections

Synthesis

LFP/C-P composites were successfully synthesized via a simple sol-gel method in this paper. The stoichiometric raw materials of Li_2CO_3 (Merck, min. 99%), $\text{Fe}_3(\text{PO}_4)_2$ (Fluka, min. 98%), $\text{NH}_4\text{H}_2\text{PO}_4$ (Merck, min. 99%), and triphenylphosphine ($\geq 99\%$, Sigma-Aldrich) were dissolved in deionized water to form a mixed salt solution. A certain amount of citric acid was added as the complexing agent for the gel, and 7 wt% graphite was added as the carbon source. Combination of these different materials can form a multidimensional interconnected conducting carbon network for LIB cathode and further improve the performance of LFP composite material. The mixed solutions were sonicated for 3 h in an ultrasonic processor and stirred vigorously under 80°C . The precursor was dried thoroughly and then heat treated in a tube furnace at 350°C for 5 h under steadily flowing nitrogen atmosphere. Afterward, the loose precursors were further sintered at 700°C for 10 h in the tube furnace with a stream of the same atmosphere. A heating rate of 2°C min^{-1} and a natural cooling in the furnace were adopted in the calcination process. LFP/C-P composites were obtained as the tube furnace cooled to room temperature. LFP/C was synthesized with the same pattern except triphenylphosphine and LFP-P was manufactured with the same approach deducted graphite. Pure LFP was prepared by a simple sol-gel reaction method without adding graphite as the carbon source and triphenylphosphine as the phosphorus source.

As shown in the Fig. 1 below, it is a schematic diagram of the synthesized LFP/C-P composite cathode materials based

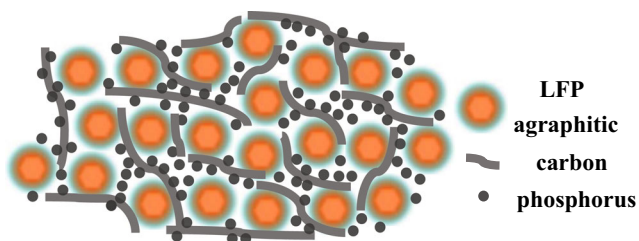


Fig. 1 A schematic diagram of the synthesis distribution of LFP/C-P composite cathode

on phosphorus doped graphite network structure. It can be shown clearly that the LFP particles are wrapped tightly in spider net-like membrane networks. Therefore, it just looks like a passion fruit, and many little LFP particles are seeds of the watermelon, while the phosphorus just like sarcocarp of the watermelon which is comparatively dispersive and ruleless, and carbon generated by graphite vividly like wrinkled texture and tortuous vein. Then, LFP/C-P composite cathode materials show an improved electrochemical performance by in situ phosphorus doped with hierarchical porous graphite-like mutual inosculating network [22].

Cell preparation

The CR2025 coin cells were made to test electrochemical performance using lithium sheet as the anode material and the above prepared electrode sample as the cathode material. The cathode materials of the cells were made from a slurry containing 80 wt% active phosphate material, 10 wt% conductive acetylene black as a conductive agent, and 10 wt% polyvinylidene fluoride (PVDF) as a binder dissolved in *n*-methyl pyrrolidinone. And, the mixed slurry was evenly spreading onto an aluminum foil then drying in a vacuum box at 120 °C more than 15 h. The electrolyte comprises 1 mol L⁻¹ LiPF₆ in a mixture of ethylene carbonate (EC) and dimethyl carbonate (DMC) with a ratio of 1:1 by volume. The fastener-like cell was assembled in an argon atmosphere glove box, where H₂O and O₂ content were not more than 0.1 ppm, and a thin sheet of microporous polyethylene (Celgard, K-849) separated the anode from the cathode. Experimental cells were tested charging-discharging performance on a LAND-CT2001A tester (Wuhan, China) with the voltage range of 2.7–4.2 V at room temperature.

Results and discussion

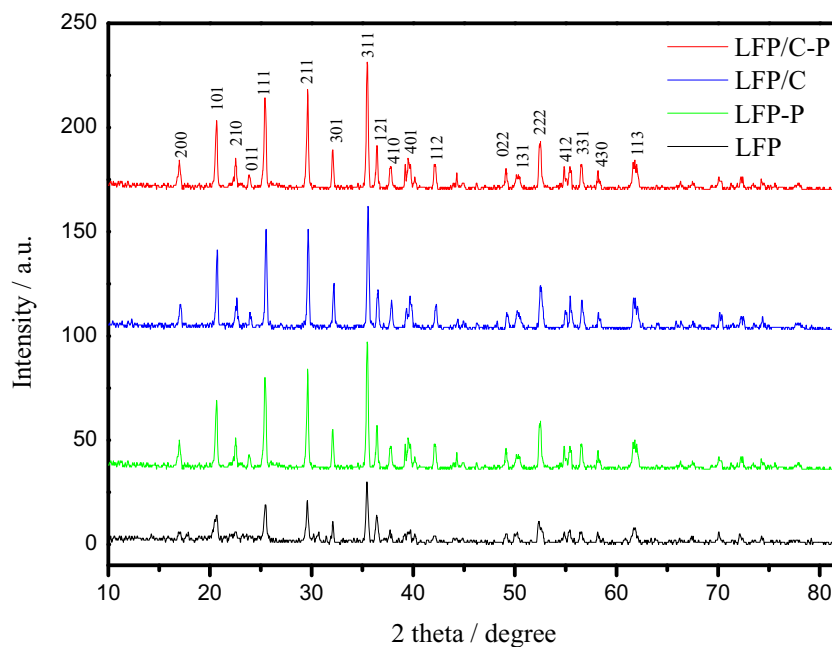
The XRD patterns of LFP, LFP-P, LFP/C, and LFP/C-P composite cathode materials are clearly shown above as Fig. 2. Obviously, the obvious diffraction peaks of the four samples can be correctly corresponded to single-phase LFP with an ordered orthorhombic olivine structure with space group Pnma. According to the XRD patterns, there is no evidence

for the formation of crystalline or amorphous carbons. It is clearly found that there is no extra diffraction peak appearance of a second phase, indicating that all the LFP cathode material samples have the pure crystallinity and excellent phase purity. Possibly, a little thin layer of residual carbon on the LFP cannot be discerned by XRD spectrogram [23]. It is obvious that doping phosphorus has no obvious effect on the structure of the samples. Strictly speaking, Fe²⁺ will be changed to Fe³⁺ with a smaller radius during de-intercalation, which makes the channels wider, and thus, the Li⁺ can move across the channels easily [24]. Moreover, from LFP to LFP/C-P, the diffraction peaks become wider with the introduction of carbon and phosphorus. In addition, there are no typical diffraction peaks of carbon, suggesting that coating carbon exists as an amorphous form.

The electrochemical performance of the materials is closely related to their chemical and physical properties, such as the particle size, surface topography, structural integrity, and surface distribution of the materials. The SEM images indicate that all the samples are composed of numerous spherality-like particles with a diameter of ~ 100 to 200 nm (Fig. 3a–d), and the interconnected channel distributes evenly around the original nanoparticles [25]. Figure 3a1, a2 shows the SEM images of the bare LFP sample. Obviously, the pure LFP shows an uneven particle size range of 100–200 nm with several clear block, broad size region, and massive agglomerations, which maintains the spherical morphology and particle size of Fe₃(PO₃)₂ precursor [26]. Afterwards, from the SEM images of LFP-P in Fig. 3b, the spider net-like carbon membrane does not emerge, and the LFP particles are still tightly agglomerated by an uneven coating layer. However, doping phosphorus leads to the smaller LFP particle size and interconnected LFP particle distribution, which is good for Li⁺ diffusion and cycling performance. Figure 3c demonstrates that the interlaced graphite, embedded and incorporated into the LFP particles intimately, reduces the agglomeration and particles sizes, which could significantly strengthen electrical conductivity of the composite electrode. SEM images of the LFP/C-P composite cathode material are shown in Fig. 3d. Obviously, the LFP particles are well spread on carbon support network doped phosphorus. In fact, interconnected channel structure of LFP/C-P composite particle suggests small diffusion length and large surface reaction sites for Li⁺, which can enhance the Li⁺ intercalation kinetics and improve the electrochemical performance of materials [27]. The interconnected channel structure is what we anticipated because the small LFP particle leads to the reduction of diffusion path of Li⁺ and the enhancement of diffusion speed. As a result, the LFP/C-P composites exhibit an increased electrochemical performance.

TEM measurement was utilized for the further observation of the morphology and microstructure of the as-prepared composites. Figure 4 shows the TEM images of the prevent synthesized LFP, LFP-P, LFP/C, and LFP/C-P composites,

Fig. 2 X-ray diffraction patterns (XRD) of LFP materials prepared by LFP, LFP-P, LFP/C, and LFP/C-P



and it is obvious that all the samples were composed of nanocrystalline particles. As shown in Fig. 4a, the bare LFP exhibits micron-sized bulk morphology with good crystallinity. Additionally, it is believed that the uniform morphology and small size of the LFP particles are favorable for the intercalation of Li^+ [28]. Thus, the decrease of LFP particle size results in the increased repulsion between Li^+ and Fe^{2+} cations, and the reduced strength of Li-O bonds results in the lower activation energy and enhanced conductivity [29].

Figure 4b presents the distribution of LFP grains with doping phosphorus. It can be seen that the carbon phosphorus compounds are well dispersed between LFP grains. However, doping phosphorus does not affect the structure and pattern of the pure LFP. It has been suggested that prior synthesized smaller particles of LFP are helpful for the accessibility of Li^+ to the redox center, resulting in a lower polarization and a higher reversible capacity [30].

LFP/C composite was prepared by only adding graphite as carbon source. It can be shown in Fig. 4c that the LFP/C granules were coated with a thin uneven film of the carbon layers. The conductive carbon coating on the surface of LFP particles can reduce the massive agglomerations of particles and the contact resistance of particle to particle evidently, and enhanced its electrical conductivity significantly [31].

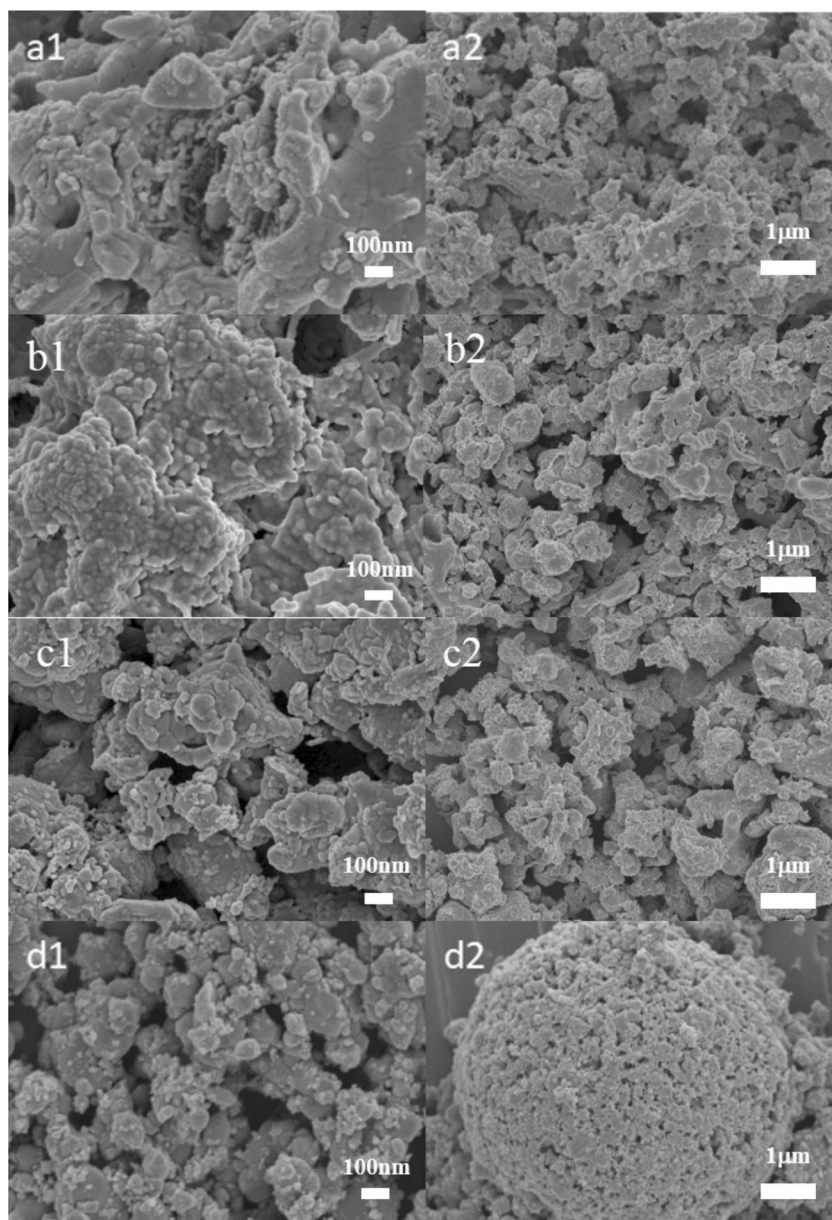
As shown in Fig. 4d, complex carbon exists in the form of amorphous carbon with excellent conductivity and phosphorus doped carbon layer can easily form a new accessible conductive network between particles of materials in a “bridging” manner. It can ensure the synchronization of charge and discharge state between the electrode surface and the inner particle effectively, thus avoiding the solution of transition metal ions caused by local overcharging. This interconnected

network channel structure of LFP by carbon nanometer canal is expected to enhance the efficient electron transfer in the cathode layer [32]. A carbon network organization becomes clear in the median granulum boundary zone, which could explain the electrical connection between LFP/C-P grains and improve its surface electrical conductivity. Meantime, the inherent electrical conductivity of LFP/C-P is boosted by the phosphorus doping.

Selecting a point randomly in a TEM image to analyze, the EDX and elemental mapping of LFP/C-P composite cathode were performed and the results are presented in Fig. 5, which shows composition content and distribution of all elements in the material and three relevant EDX maps of phosphorous, iron, and oxygen in LFP/C-P composite cathode. Obviously, it can be seen that all elements have monotonous coincident distribution in the mapping spectrogram, indicating that the carbon and phosphorus combined uniformly with LFP granules and the carbon network interconnected channel structure is dispersed evenly among the LFP particles [33].

Figure 6 shows the initial charge/discharge extents of the four samples under a voltage range of 2.7–4.2 V at 0.1 C. All samples have a palpable discharge plateaus at 3.4–3.5 V due to the two phases of FePO_4 and LFP with redox reaction. Ordinarily, the sample with higher discharge plateaus and availability efficiency can lengthen working time for electronic equipments. In the first cycle at 0.1 C, the discharge capacities of LFP, LFP-P, LFP/C, and LFP/C-P composite cathode material are 121.5, 144.2, 147.0, and 165.3 mAh g^{-1} , and the capacity retention are 98.5%, 98.7%, 93.6%, and 99.9%, severally. LFP/C-P composite shows the highest discharge plateau, suggesting that the doped phosphorus into carbon net can significantly enhance cathode materials with excellent

Fig. 3 SEM images of LFP (a), LFP-P (b), LFP/C (c), and LFP/C-P (d)

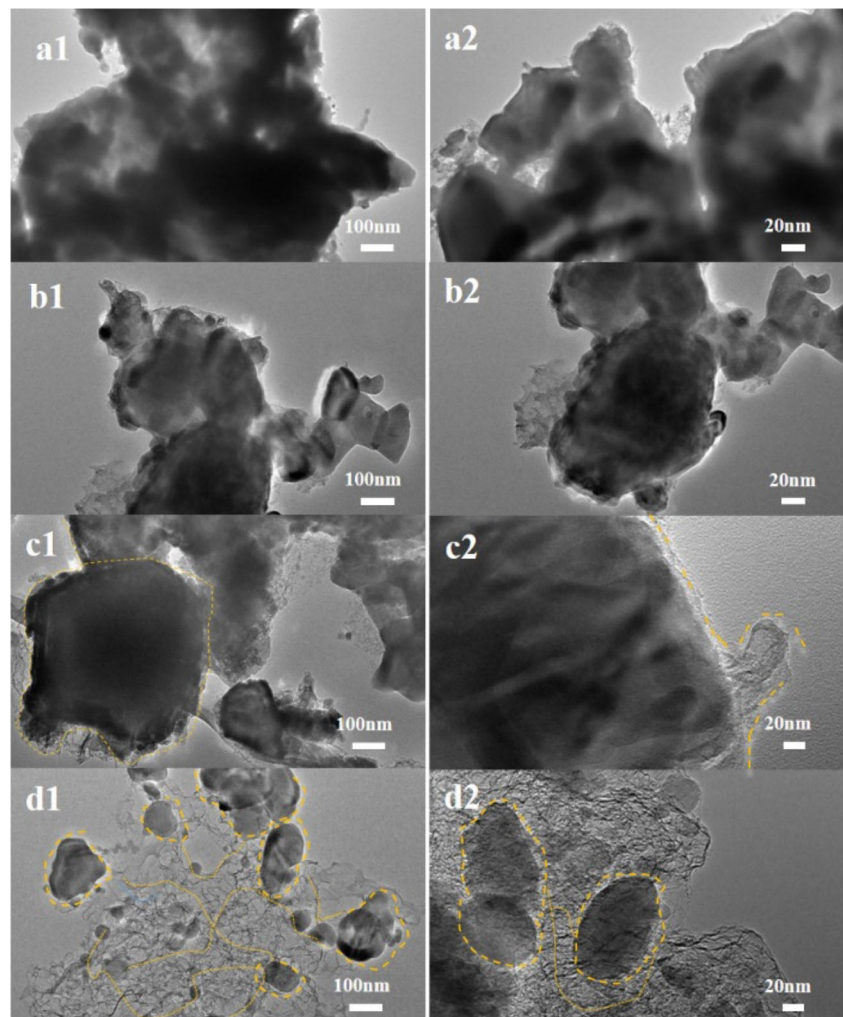


specific capacities and stable coulombic efficiency [34]. It can be seen that the polarization of LFP/C-P sample is smaller, and the discharge capacity is higher. The possible reason is that LFP/C-P particles have the advantages of interconnected structure by carbon nanometer channel compared with LFP, which is conducive for the better contact between the electrolyte and materials. The full contact between cathode and electrolyte results in the reduced diffusion resistance and shorter Li^+ diffusion path. As a result, the acceleration of the transmission of Li^+ improves ionic conductivity and the utilization rate of the material [35].

In order to investigate the rate capability of LFP, LFP-P, LFP/C, and LFP/C-P composite cathode, the cells were charged/discharged at various rates from 0.1 to 5 C rates, progressively. Figure 7 represents the site-dependent charge/

discharge curves of LFP, LFP-P, LFP/C, and LFP/C-P samples at different cycle rates. The discharge capacities of LFP/C-P sample were 165.6 mAh g^{-1} , 154.7 mAh g^{-1} , 145.3 mAh g^{-1} , 128.5 mAh g^{-1} , and 106.4 mAh g^{-1} when it was discharged under 0.1 C, 0.5 C, 1.5 C, 3 C, and 5 C, respectively. The higher discharge capacity of LFP/C-P material can be illustrated as that phosphorus doping is conducive to form a new efficient conductive network between particles of materials by building an amount of interconnected “bridges” [36]. The refined structure would be effective for reducing the diffusion distance of Li^+ ; thus, the Li^+ diffusion speed and discharge capacity would be strengthened. And, apparently, with the increase of rate, the capacity attenuation of all samples decay obviously and the capacity retention of LFP/C-P are better than the others [37]. The results show that the electrochemical

Fig. 4 TEM images of LFP (a), LFP-P (b), LFP/C (c), and LFP/C-P (d)



performance of the LFP/C-P composite cathode materials can be improved significantly by appropriate adjunction of carbon and phosphorus.

The cycling properties of all samples are examined at the rate of 0.1 C for 100 cycles. As marked in Fig. 8, the slight increase of capacity of LFP and LFP/C-P samples in the first

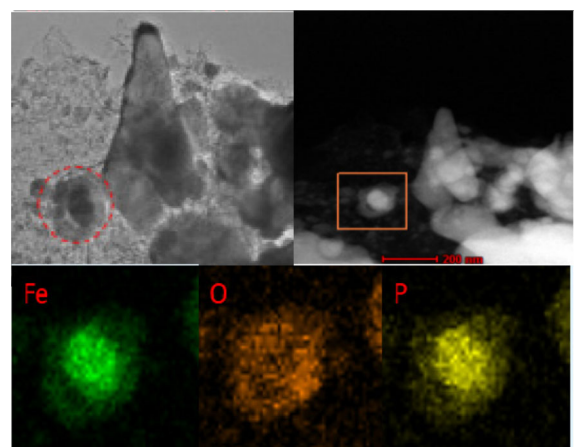
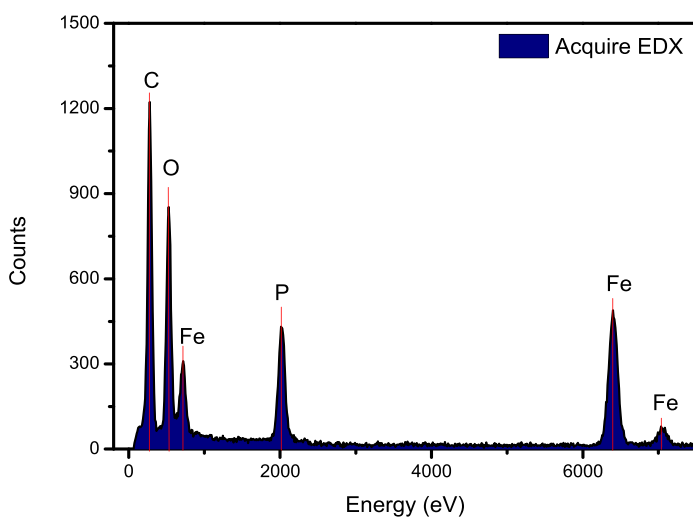


Fig. 5 EDX and elemental mapping for the particles of the LFP/C-P composite cathode

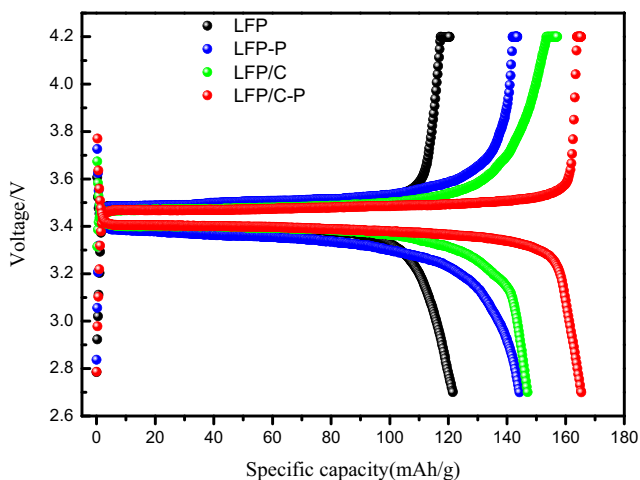


Fig. 6 First charge-discharge profile of LFP, LFP-P, LFP/C, and LFP/C-P at 0.1 C

few cycles is usually attributed to slow penetration of electrolyte into micro-particles. Obviously, the LFP/C-P electrode represents a lower capacity fading and a better cycle stability at 0.1 C compared with other three samples. The capacity fading of the LFP, LFP/C, and LFP-P is attributed to the sluggish diffusion of Li^+ and the larger polarization [38]. The reticulated particle distribution of LFP/C-P sample, showing little polarization, not only achieved higher initial discharge capacity but also kept more cycle retention. In addition, the LFP/C-P shows outstanding reversal capacity performance with little diminution of capacity at each current density, which also confirms the results of XRD and TEM mentioned above with the phosphorus-doped carbon network structure [39].

EIS was applied to further investigate the efficacy of alien metal occupied site on the electrode impedance. The complex impedance plots are obtained with electrodes based on all the four samples upon EIS experiments performed at discharged state that have been analyzed by fitting the curves to a model.

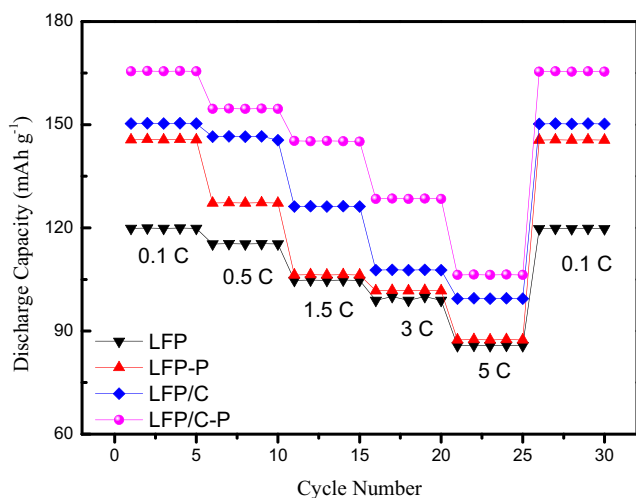


Fig. 7 Rate performance of LFP cells of LFP, LFP-P, LFP/C, and LFP/C-P

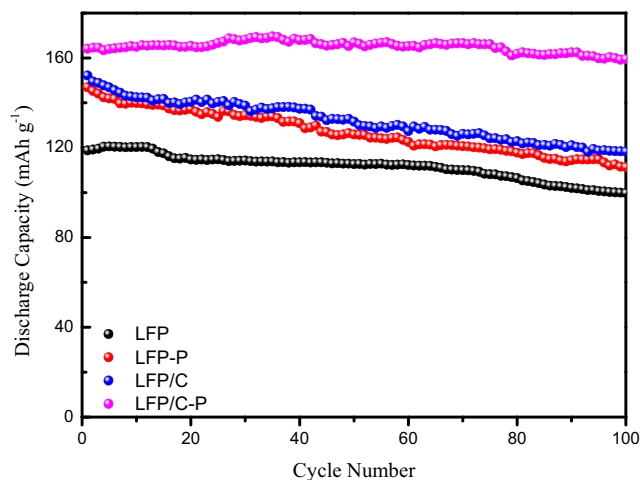


Fig. 8 Cycle performances of LFP, LFP-P, LFP/C, and LFP/C-P with 0.1 C charge/discharge rate at room temperature

Figure 9 shows the Nyquist plots of discharged LFP, LFP-P, LFP/C, and LFP/C-P samples after 3 cycles, where R_s indicates the electrolyte solution resistance, R_{ct} represents the charge transfer resistance on account of the diameter of the semicircle at high frequency, and the Warburg resistance (R_w) corresponds to the inclined line [40]. It can be seen that each plot consists of a semicircle at the high frequency region and a sloping line at the low-frequency area. The semicircle in the high-frequency region corresponds to the impedance of charge transfer (R_{ct}) due to the diffusion of Li^+ ion in the electrode/electrolyte interface via the SEI layer, and the semicircle at mid frequency region is the charge-transfer resistance [41]. Moreover, the straight line in low-infrequency region represents the Warburg impedance due to the diffusion of Li^+ in the surface of electrode materials. The cell impedance mostly depends on R_{ct} , and the values of R_{ct} are 35.5 Ω for LFP/C-P and 68.2 Ω , 152.3 Ω , and 371.8 Ω for LFP, LFP-P, and LFP/C, severally. It can be seen that the R_{ct} of LFP/C-P is

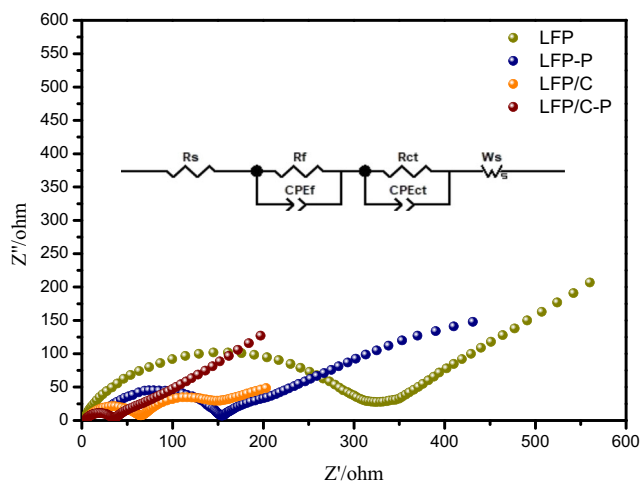


Fig. 9 Electrochemical impedance spectra (EIS) of LFP, LFP-P, LFP/C, and LFP/C-P

smaller than others, indicating that LFP/C-P is favorable to the charge transfer due to its stable interconnected bridges structure [42]. On the basis of previous research reports, it can be concluded that the LFP/C-P samples have the optimal electrochemical performance. The lithium ion diffusion coefficients (D) are calculated according to the following equation:

$$D = \frac{R^2 T^2}{2A^2 n^4 F^4 C^2 \sigma^2}$$

where R is the gas constant, T is the absolute temperature, A is the surface area of the cathode, n is the number of electrons per molecule during oxidization, F is the Faraday constant, C is the concentration of lithium ion, and σ is the Warburg factor which is relative with reciprocal square root of frequency in the low-frequency region. The calculated lithium ion diffusion coefficients of LFP, LFP-P, LFP/C, and LFP/C-P are 9.73×10^{-14} , 1.13×10^{-13} , 1.56×10^{-13} , and 1.78×10^{-13} $\text{cm}^2 \text{s}^{-1}$, respectively, suggesting that the phosphorus-doped sample LFP/C-P is more flexible for the diffusion of lithium ions and thus has a better electrochemical performance than other

samples. Therefore, the EIS analysis further confirms that the phosphorus-doped carbon coating is effective in improving the electrical conductivity of LFP.

In addition, the XPS spectra of LFP, LFP-P, LFP/C, and LFP/C-P samples were tested to determine the state of phosphorus existed in the electrode material compound. As shown in Fig. 10, the pure LFP, uncoated LFP-P, and undoped LFP/C samples all present two peaks approximately at 131.58 ± 0.2 eV and 132.48 ± 0.3 eV, which suggests the bijection of the P–O and P=O chemical bonds. However, a new small unique peak just emerged at 131.98 eV for LFP/C–P, which proved the emerging of P–C chemical bonds. Neither the LFP-P sample prepared by adding phosphorus alone nor the LFP/C sample prepared by adding carbon alone has this special peak in the XPS spectra, which means that P–C bond can only be formed by the combination of additional phosphorus and graphite [43].

Figure 11 shows the cyclic voltammetry (CV) curves of the samples after several cycles. It can be observed that the oxidation peaks and reduction peaks of the materials are approximately symmetrical, which means great reversibility of the

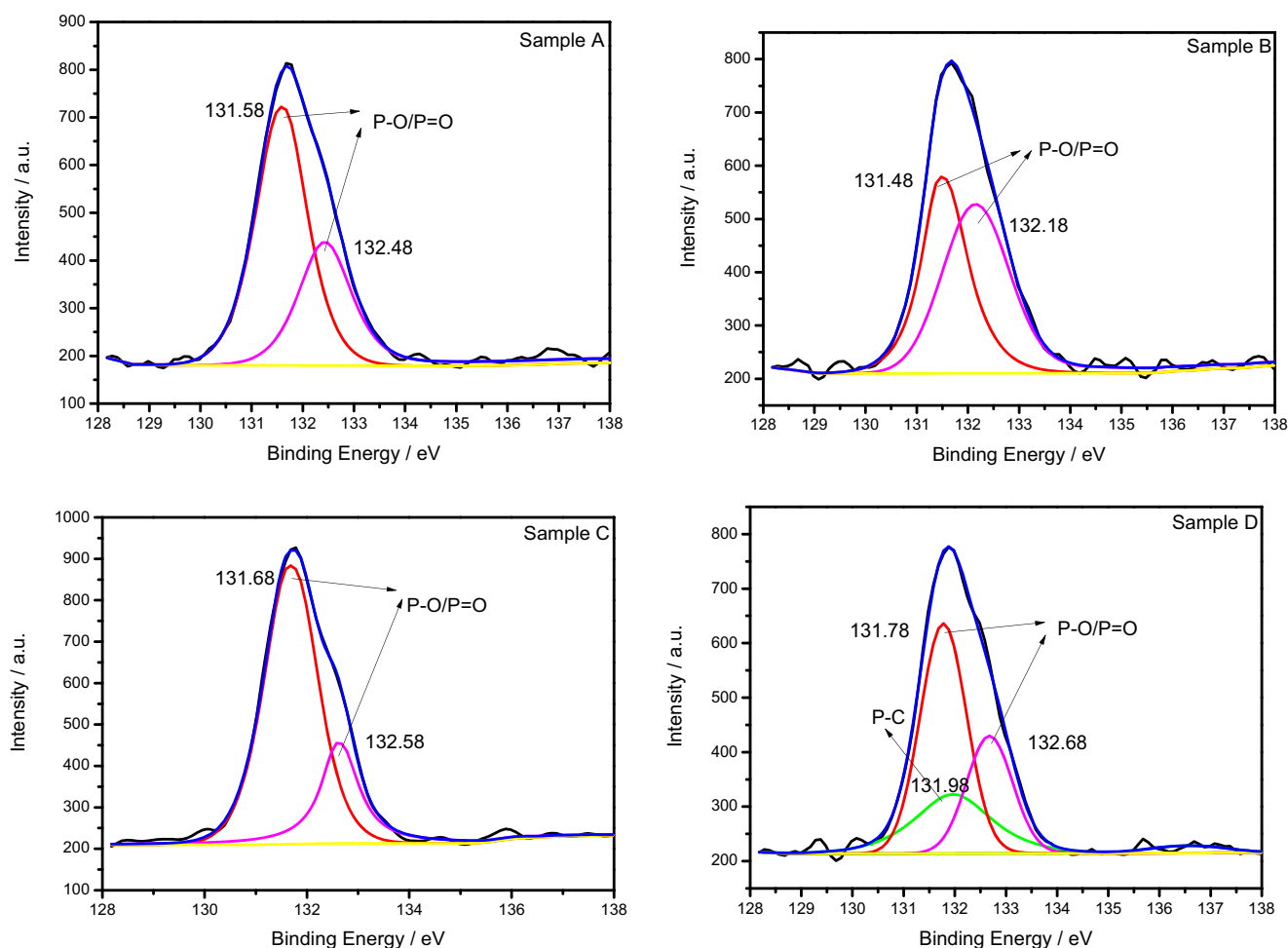


Fig. 10 XPS spectra of P 2p of LFP, LFP-P, LFP/C, and LFP/C-P

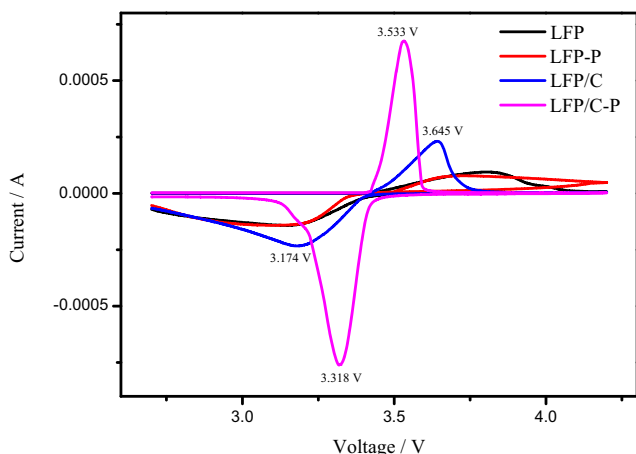
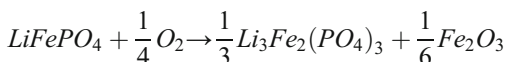


Fig. 11 Cyclic voltammetry (CV) curves of LFP, LFP-P, LFP/C, and LFP/C-P

Li⁺ insertion/extraction. Furthermore, the potential gaps ($\Delta V = 0.115$ V) of LFP/C-P is much smaller than that of others, indicating a lower polarization owing to the addition of carbon and phosphorus. LFP/C-P sample exhibits sharpest oxidation and reduction peaks, displaying best kinetic properties during the redox process of the four samples.

TGA of LFP and LFP/C-P is conducted to estimate the carbon and graphene content under a flowing air atmosphere, and the curves are shown in Fig. 12. For LFP, the TGA curve reveals a weight gain of approximately 1.9 wt%. This can be explained by the following oxidation reaction:



However, the increase in the LFP of approximately 1.9% is below the theoretical increase of 5%, which may arise from the presence of oxalate and carbonate in the precursors, resulting in a carbon residue in the solid phase reaction. The weight of LFP/C-P is lost owing to the oxidation of carbon

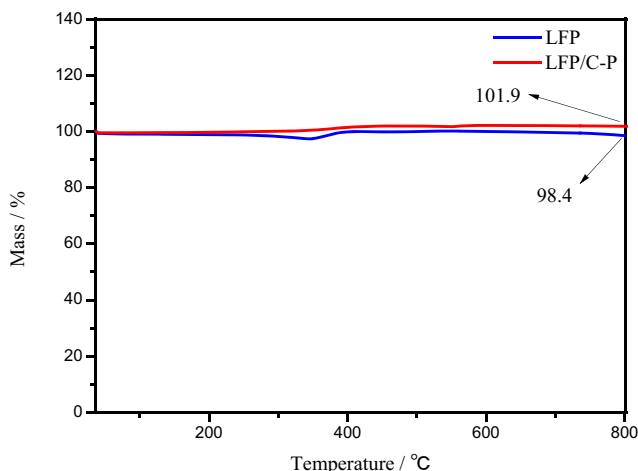


Fig. 12 TGA curves of LFP and LFP/C-P samples

under a flowing air atmosphere. The weight change of LFP/C-P is approximately 1.6%. Therefore, the amount of carbon coated on LFP for LFP/C-P is approximately 3.5%.

Therefore, it can be concluded that both the carbon network and doped phosphorus on the LFP particles are critical for the success of the LFP/C-P composite cathode, and no one can be omitted. On one hand, the carbon network not only enhances the decentralization of phosphorus in the LFP particles but also provides a beneficial electronic contact between the oxide particles and current collector. On the other hand, doping phosphorus promotes the final formation of carbon network linking LFP particles with a large number carbon nanometer channel [44]. However, it is still unclear what form of phosphorus is present in the composite and it is also one of the key points that continuing to study in depth.

Conclusions

In summary, a lower energy-consumption and easy scaled-up procedure has been developed for fabricating LFP/C-P composite cathode material with great electrochemical performance for lithium ion batteries. The optimal LFP/C-P composite cathode material shows a high capacity of 168.8 mAh g⁻¹ at 0.1 C and still keeps predominant cycling stability after 100 cycles. The remarkable electrochemical behavior is attributed to the unique spider network structure, where the three-dimensional carbon network channel serves as an efficient link media for electron transport. The enhanced electrochemical performance of LFP/C-P composite cathode material could be mainly attributed to the synergetic effect of bridging graphite nanometer nets and forming an interconnected conducting network with cross linking between many neighboring LFP particles. This special network could improve the cycle stability of the LFP composite and accelerate the exchange movement during charge/discharge cycling.

The modification of LFP/C-P composite cathode material by carbon and phosphorus conductive network can overcome the disadvantage of long Li⁺ transport path caused by large particles and further promote the specific capacity, rate performance, and structural stability of the cathode material. In addition, it is also necessary to continue to study in depth the mechanism and influence of carbon and phosphorus in the conductive network, such as the type, calcination temperature, time, and atmosphere of the raw materials.

Funding information This work is supported by the Natural Science Foundation of China (No. 21566021 and 21766017), the Transformation of Scientific and Technological Achievements of Gansu Institutions of Higher Education (No. 2017D-04), and the Supporting Plan for Youth Innovative Talents of Longyuan.

References

- Halankar KK, Mandal BP, Jangid MK, Mukhopadhyay A, Meena SS, Acharya R, Tyagi AK (2018) Optimization of lithium content in LiFePO₄ for superior electrochemical performance: the role of impurities. *RSC Adv* 8:1140–1147
- Lewerenz M, Marongiu A, Warnecke A, Sauer DU (2017) Differential voltage analysis as a tool for analyzing inhomogeneous aging: a case study for LiFePO₄/graphite cylindrical cells. *J Power Sources* 368:57–67
- Zhang C, Yan F, Du C et al (2017) Evaluating the degradation mechanism and state of health of LiFePO₄ lithium-ion batteries in real-world plug-in hybrid electric vehicles application for different ageing paths. *Energies* 10:110–123
- Zhang Y, Xin P, Yao Q (2018) Electrochemical performance of LiFePO₄/C synthesized by sol-gel method as cathode for aqueous lithium ion batteries. *J Alloys Compounds* 741:404–408
- Huang J, Wang J, Zhong H, Zhang L (2018) N-Cyanoethyl polyethylenimine as a water-soluble binder for LiFePO₄ cathode in lithium-ion batteries. *J Mater Sci* 53:9690–9700
- He J, Zhong H, Zhang L (2018) Water-soluble binder PAAli with terpene resin emulsion as tackifier for LiFePO₄ cathode. *J Appl Polym Sci* 135:46132–46138
- Fischer MG, Hua X, Wilts BD, Castillo-Martínez E, Steiner U (2018) Polymer-templated LiFePO₄/C nanonetworks as high-performance cathode materials for lithium-ion batteries. *ACS Appl Mater Interfaces* 10:1646–1652
- Chen YT, Zhang HY, Chen YM, Qin G, Lei XL, Liu LY (2018) Graphene-carbon nanotubes-modified LiFePO₄ cathode materials for high-performance lithium-ion batteries. *Mater Sci Forum* 913: 818–830
- Zhang H, Chen Y, Zheng C, Zhang D, He C (2015) Enhancement of the electrochemical performance of LiFePO₄/carbon nanotubes composite electrode for Li-ion batteries. *Ionics* 21:1813–1818
- Qiu S, Zhang X, Li Y, Sun T, Wang C, Qin C (2016) Facile synthesis and electrochemical performances of secondary carbon-coated LiFePO₄-C composite for Li-ion capacitors based on neutral aqueous electrolytes. *J Mater Sci Mater Electron* 27:7255–7264
- Seo JH, Verlinde K, Guo J, Heidary DSB, Rajagopalan R, Mallouk TE, Randall CA (2018) Cold sintering approach to fabrication of high rate performance binderless LiFePO₄ cathode with high volumetric capacity. *Scr Mater* 146:267–271
- Wei X, Guan Y, Zheng X, Zhu Q, Shen J, Qiao N, Zhou S, Xu B (2018) Improvement on high rate performance of LiFePO₄ cathodes using graphene as a conductive agent. *Appl Surf Sci* 440:748–754
- Anseán D, Dubarry M, Devie A, Liaw BY, García VM, Viera JC, González M (2017) Operando lithium plating quantification and early detection of a commercial LiFePO₄ cell cycled under dynamic driving schedule. *J Power Sources* 356:36–46
- Madram AR, Daneshalab R, Sovizi MR (2016) Effect of Na⁺ and K⁺ co-doping on the structure and electrochemical behaviors of LiFePO₄/C cathode material for lithium-ion batteries. *RSC Adv* 6: 101477–101484
- Oh J, Lee J, Hwang T, Kim JM, Seoung KD, Piao Y (2017) Dual layer coating strategy utilizing N-doped carbon and reduced graphene oxide for high-performance LiFePO₄ cathode material. *Electrochim Acta* 231:85–93
- Naumann M, Schimpe M, Keil P, Hesse HC, Jossen A (2018) Analysis and modeling of calendar aging of a commercial LiFePO₄/graphite cell. *J Energy Storage* 17:153–169
- Gúeguen A, Castro L, Dedryvère R et al (2017) The electrode/electrolyte reactivity of LiFe_{0.33}Mn_{0.67}PO₄ compared to LiFePO₄. *J Electrochem Soc* 160:A387–A393
- Wang P, Zhang G, Li Z et al (2016) Improved electrochemical performance of LiFePO₄@N-doped carbon nanocomposites using polybenzoxazine as nitrogen and carbon sources. *ACS Appl Mater Interfaces* 8:141–149
- Xiao P, Henkelman G (2018) Kinetic Monte Carlo study of Li intercalation in LiFePO₄. *ACS Nano* 12:844–851
- Panchal S, Dincer I, Agelin-Chaab M, Fowler M, Fraser R (2017) Uneven temperature and voltage distributions due to rapid discharge rates and different boundary conditions for series-connected LiFePO₄ batteries. *Int J Heat Mass Transfer* 81:210–217
- Jung WK, Baek C, Kim JH, Moon S, Kim DS, Jung YH, Kim DK (2018) A highly-aligned lamellar structure of ice-templated LiFePO₄ cathode for enhanced rate capability. *Mater Des* 139:89–95
- Gao L, Xu Z, Zhang S, Xu J, Tang K (2017) Enhanced electrochemical properties of LiFePO₄ cathode materials by Co and Zr multi-doping. *Solid State Ionics* 305:52–56
- Lachal M, Bouchet R, Boulineau A, Surblé S, Rossignol C, Alloin F, Obbade S (2017) Remarkable impact of grains boundaries on the chemical delithiation kinetics of LiFePO₄. *Solid State Ionics* 300: 187–194
- Tong B, Wang J, Liu Z, Ma L, Zhou Z, Peng Z (2018) Identifying compatibility of lithium salts with LiFePO₄ cathode using a symmetric cell. *J Power Sources* 384:80–85
- Chen M, Kou K, Tu M, Hu J, du X, Yang B (2017) Conducting reduced graphene oxide wrapped LiFePO₄/C nanocrystal as cathode material for high-rate lithium secondary batteries. *Solid State Ionics* 310:95–99
- Zhu J, Sun Z, Wei X, Dai H (2017) Battery internal temperature estimation for LiFePO₄ battery based on impedance phase shift under operating conditions. *Energies* 10:60–77
- Feng W (2017) Effect of carbon nanotubes on the electrochemical performance of LiFePO₄ particles in lithium ion batteries. *Int J Electrochem Sci* 10:5199–5207
- Choi H, Kim HJ, Shim IB, Lee IK, Kim CS (2017) Structural and magnetic properties of lithium cathode materials Li_xFe_{1/3}Co_{1/3}Ni_{1/3}PO₄ (x = 0, 1). *Mater Res Bull* 93:361–365
- Wu G, Liu N, Gao X, Tian X, Zhu Y, Zhou Y, Zhu Q (2018) A hydrothermally synthesized LiFePO₄/C composite with superior low-temperature performance and cycle life. *Appl Surf Sci* 435: 1329–1336
- Yuksel T, Litster S, Viswanathan V, Michalek JJ (2017) Plug-in hybrid electric vehicle LiFePO₄ battery life implications of thermal management, driving conditions, and regional climate. *J Power Sources* 338:49–64
- Sood R, Jojoiu C, Espuche E et al (2017) Proton conducting ionic liquid doped nafion membranes: nano-structuration, transport properties and water sorption. *J Physical Chem C* 116:24413–24423
- Lewerenz M, Münnix J, Schmalstieg J, Käbitz S, Knips M, Sauer DU (2017) Systematic aging of commercial LiFePO₄/graphite cylindrical cells including a theory explaining rise of capacity during aging. *J Power Sources* 345:254–263
- Chaoui H, Ibe-Ekeocha CC, Gualous H (2017) Aging prediction and state of charge estimation of a LiFePO₄ battery using input time-delayed neural networks. *Electr Power Syst Res* 146:189–197
- Johnson ID, Ashton TE, Blagovidova E, Smales GJ, Lübke M, Baker PJ, Corr SA, Darr JA (2018) Mechanistic insights of Li⁺ diffusion within doped LiFePO₄ from muon spectroscopy. *Sci Rep* 8:4114–4120
- Tian X, Zhou Y, Tu X, Zhang Z, du G (2017) Well-dispersed LiFePO₄ nanoparticles anchored on a three-dimensional graphene aerogel as high-performance positive electrode materials for lithium-ion batteries. *J Power Sources* 340:40–50
- Wu YJ, Gu YJ, Chen YB, Liu HQ, Liu CQ (2018) Effect of lithium phosphate on the structural and electrochemical performance of

- nanocrystalline LiFePO_4 , cathode material with iron defects. *Int J Hydrog Energy* 43:2050–2056
37. He L, Zha W, Chen D (2017) Effects of organic phosphorus acid on the core-shell structure and electrochemical properties of LiFePO_4 uniformly wrapped with in-situ grown graphene nanosheets. *J Alloys Compounds* 727:948–955
 38. Kim MS, Lee GW, Lee SW et al (2017) Synthesis of LiFePO_4 /graphene microspheres while avoiding restacking of graphene sheet's for high-rate lithium-ion batteries. *J Ind Eng Chem* 4(52): 251–259
 39. Du Y, Tang Y, Chang C (2017) Enhanced electrochemical performance from 3DG/ LiFePO_4 /G sandwich cathode material. *J Phys Chem Solids* 107:36–41
 40. Xiong QQ, Lou JJ, Teng XJ, Lu XX, Liu SY, Chi HZ, Ji ZG (2018) Controllable synthesis of N-C@ LiFePO_4 , nanospheres as advanced cathode of lithium ion batteries. *J Alloys Compounds* 743:377–382
 41. Bao L, Xu G, Sun X, Zeng H, Zhao R, Yang X, Shen G, Han G, Zhou S (2017) Mono-dispersed LiFePO_4 @C core-shell [001] nanorods for a high power Li-ion battery cathode. *J Alloys Compounds* 708:685–693
 42. Okada K, Kimura I, Machida K (2018) High rate capability by sulfur-doping into LiFePO_4 matrix. *RSC Adv* 8:5848–5853
 43. Eftekhari A (2017) LiFePO_4 /C nanocomposites for lithium-ion batteries. *J Power Sources* 343:395–411
 44. Gao Z, Cheng C, Woo W et al (2017) Integrated equivalent circuit and thermal model for simulation of temperature-dependent LiFePO_4 battery in actual embedded application. *Energies* 10:85–107